International Journal of Mechanical Engineering and Robotics Research Vol. 4, No. 4, October 2015

Camera-Based Field of View Parameter Optimization

Marek Steß
Volkswagen AG Group Research, Germany
Email: marek.stess@volkswagen.de

Michael Schlichte and Bernardo Wagner
c4c Engineering GmbH, Brunswick, Germany and Leibniz Universität Hannover, Hanover, Germany
Email: michael.schlichte@c4cengineering.de, wagner@rts.uni-hannover.de

***Abstract*—Nowadays cars are equipped with more and more sensors to be able to drive autonomously. Soon cars will become service robots which require a precise self localization. But instead of interacting in a goodwill environment like offices, hallways or warehouses, automated cars will be interacting in the real world. Hence they have to handle different types of challenges like seasonal and structural change, changing lighting, and weather conditions. These atmospheric conditions influence the required precise self localization. Therefore this paper introduces a method to generate weather specific field of view parameters for dashed road marking landmarks extracted by a mono camera. With these parameter sets a useful reduction of the measurement set is achieved. This should lead to an improvement of the localization accuracy compared with standard field of view parameters. To this end, we examine three atmospheric conditions: rain, wetness and dryness.**

***Index Terms*—localization, fuzzy learning, landmark based localization, field of view, atmospheric conditions, weather conditions**

I. Introduction

Fully automated driving systems need a localization module with a precision of few centimeters. Scenarios like lane changing, cross ways, and overtaking maneuvers require such a high degree of precision.

Nowadays common localization methods for automated driving differentiate between mapping as well as localization and treat both in isolation. These localization methods use a precomputed map and match current sensor observations (called measurements) into this map [1]–[10]. For this approach classified features, called landmarks, serve as measurements. Independently of the used measurements the localization global accuracy depends on the previously acquired map and the handling of measurements. Both parts affect the localization uncertainty.

In general, the domain of automated vehicles will be the real world and its systems will be confronted with different types of challenges connected with this environment, such as atmospheric conditions. Examples include heavy rain, fog, snow, and blinding effects which can negatively influence the localization.

The work in [1] for instance shows that backlighting can produce ghost landmarks or even make them unrecognizable. The authors of [8] point out that changes in the appearance of the environment, for example by changing seasons, influences the localization results.

Other authors like [1], [4] explicitly limit their localization procedure to specific weather scenarios. The authors of [11] show that lidar reflection on a wet street is not as well as on a dry one. This leads to different map qualities. A normalization of the brightness values is proposed, but this approach is not necessarily robust under all atmospheric conditions. In [12] it is shown that camera-based landmark detection works under good natured weather conditions but is strongly affected by rain. Hence a camera-based weather classification to adjust the camera perception has been introduced. Other approaches for rain detection are presented in [13]-[15].

The above mentioned approaches are not influenced by weather conditions on the localization accuracy into account. Instead localization and weather identification are treated separately. Furthermore, most publications on localization explicitly exclude bad weather conditions or build an algorithm for a single type of weather condition.

In this paper a concept on how to adjust the localization to different weather conditions is presented. The influence of these conditions on the localization precision will be addressed. In our concept an alterable field of view is used to reduce the measurement set. Different parameter sets for the field of view and their impact on the localization accuracy are analyzed. Our research examines three atmospheric conditions: rain, wetness (without rain) and dryness. We have determined different field of view parameters for each category which improve the localization. Our main contribution is to show that different field of views for the corresponding scenarios can be determined.

The remainder of this paper is organized as follows: Section II explains our localization framework and describes our modules. Afterwards we explain our optimization process for the field of view parameters and the corresponding experiments in Section III and Section

Manuscript received May 27, 2015; revised September 1, 2015.

doi: 10.18178/ijmerr.4.4.293-298

IV. Finally, Section V gives a conclusion and outlines upcoming research.

II. Localization Framework

This chapter introduces the used methods and technique. Therefore each module will be briefly described.

To run our localization framework we use mono camera images taken from a front dash camera to road markings detection. The landmark extraction module detects dashed road markings and returns these landmarks as measurements. As a consequence we get a new sample of landmarks in each detection cycle. This data contains a lot of clutter which disorder information. To reduce noise the detected measurements need to be stabilized by a tracking approach.

Based on findings in [16], the memory module has been designed to work on two layers. Its first layer statically filters length and width of the landmarks to reduce clutter. The second layer tracks the detected landmarks and calculates a belief value. The field of view is set inside this module and is used to reduce the measurement set.

The Electronic Horizon provides a map which contains road markings. The map is manually generated from WGS84 geo referenced aerial images. By sending a request with a WGS84 position, the Electronic Horizon responds with the corresponding map selection.

The association module matches the tracked landmarks of the memory into the map and recalculates the position of the car. Each dashed road marking landmark i is defined by a starting point $\vec{s}_i = (s_{xi}, s_{yi})$ and an endpoint $\vec{e}_i = (e_{xi}, e_{yi})$ in the vehicle reference frame. We differentiate between sensor landmarks L^{scan} from the memory and map landmarks L^{map} from the Electronic Horizon. Hence a landmark can by written as $\vec{L}_i^{scan}$ for a sensor landmark i in L^{scan} with starting point $\vec{s}_i^{scan}$ and ending point $\vec{e}_i^{scan}$. Map landmarks are defined likewise.

For two landmarks $\vec{L}_i^{scan}$ and $\vec{L}_j^{map}$ we calculate distances $z_{1,i,j}$ as well as $z_{2,i,j}$ and the angle α. With these results the distance function d_L returns the distance value. Equation (1) to (5) show the distance calculation. Fig. 1 introduces the described calculation, whereas part a) show two landmarks from L^{scan} and L^{map} with corresponding start points $\vec{s}_i^{scan}$, $\vec{s}_j^{map}$ and end points $\vec{e}_i^{scan}$, $\vec{e}_j^{map}$ and part b) the distances $z_{1,i,j}$, $z_{2,i,j}$ between the landmarks.

$$z_{1,i,j} = \| \vec{s}_j^{map} - \vec{s}_i^{scan} \| + \| \vec{e}_j^{map} - \vec{e}_i^{scan} \| \quad (1)$$

$$z_{2,i,j} = \| \vec{s}_j^{map} - \vec{e}_i^{scan} \| + \| \vec{e}_j^{map} - \vec{s}_i^{scan} \| \quad (2)$$

$$\angle_{i,j} = \frac{180}{\pi} \cdot \arccos \frac{\left|\vec{L}_i^{scan}\right| \cdot \left|\vec{L}_j^{map}\right|}{\left\|\vec{L}_i^{scan}\right\| \cdot \left\|\vec{L}_j^{map}\right\|} \quad (3)$$

$$\alpha = \min\left(\angle_{i,j}, 180 - \angle_{i,j}\right) \quad (4)$$

$$d_L\left(\vec{L}_i^{scan}, \vec{L}_j^{map}\right) = \sqrt{\min(z_{1,i,j}, z_{2,i,j})^2 + (0.1 \cdot \angle_{i,j})^2} \quad (5)$$

We do this for all landmarks L^{scan} within our field of view and determine thereby an assignment to the corresponding Electronic Horizon landmarks L^{map}. Therefore all distances are calculated as can be seen in (6). The corresponding map landmark $\vec{L}_j^{map}$ for a given scan landmark $\vec{L}_i^{scan}$ is identified by the lowest distance value in $A_{i,j}$ as defined in (7).

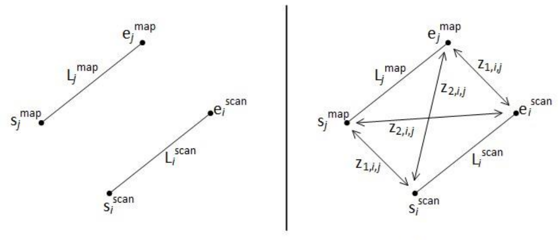

Figure 1. Distance calculation for map and scan landmarks

$$\forall\, i \in |L^{scan}|, \forall\, j \in |L^{map}| : A_{i,j} = d_L\left(\vec{L}_i^{scan}, \vec{L}_j^{map}\right) \quad (6)$$

$$d_{opt}\left(\vec{L}_i^{scan}\right) = \min_j A_{i,j} \quad (7)$$

The localization process uses a non persistent, multi hypothesis particle filter. As a characteristic of this approach particles are newly sampled in every association step. For a given input pose a fixed number of Gaussian distributed particles are generated. The association cost for each particle p_k is the sum of all single distances per scan landmark $\vec{L}_i^{scan}$ divided by their quantity as stated in (8).

$$p_k^{cost} = \frac{\sum_{i=1}^{|L^{scan}|} d_{opt}(\vec{L}_i^{scan})}{|L^{scan}|} \quad (8)$$

The particle with the lowest cost is used to calculate the corrected vehicle position.

The sensor fusion method "Localization-Sensor-DataFusion 2.0" (LSDF) [17] is used to estimate the absolute and relative position of the car by merging odometric data like the Electronic Stabilization Program (ESP) and the Antilock Braking System (ABS) with a serial car inertial measurement unit (IMU) as well as a serial GPS receiver. The calculated absolute and relative car position serves as input for the memory and association module.

The following Fig. 2 shows the described modules as an architecture overview.

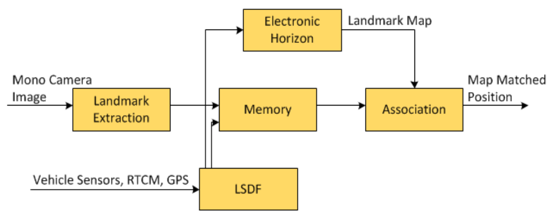

Figure 2. Localization framework

III. Impact of Field of View Variation

To evaluate whether or not different atmospheric conditions influence the localization architecture we used three categories: rain, wetness (without rain) and dryness. Fig. 3 to 5 show single images with detected landmarks for each category.

The field of view for the camera is set as an isosceles, symmetric trapeze in front of the vehicle. As the camera angle α is fixed, the distance to the bottom edge of the trapeze h_{fix} is known. The bottom vertices, equivalent to the bottom edges of the camera image, are also fixed then. However, the top vertices are adaptable. The described field of view is depicted with red stripes in Fig. 6.

According to our hypothesis the field of view can be optimized for each single category.

A parameter set $para^{set}$ consists of the total height h and a width offset w for the top vertices:

Figure 3. Rain

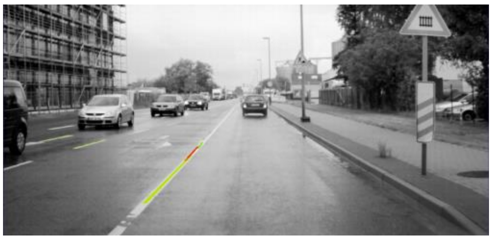

Figure 4. Wetness

Figure 5. Dryness

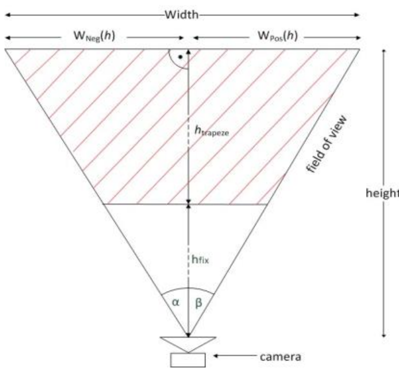

Figure 6. Field of view in red color in front of the vehicle

$$para^{set} = \left(para^{height},\ para^{with\_offset}\right) \qquad (9)$$

Thereby the total height h is defined as the trapeze height $h_{trapeze}$ plus h_{fix}. Thus, $h_{trapeze}$ is the first alterable parameter. The both alterable top vertices define the trapeze width $W(h)$ and can be calculated when the total height is known as follows:

$$W_{Neg}(h) = \left(h_{fix} + h_{trapeze}\right) \cdot \tan\alpha \qquad (10)$$

$$W_{Pos}(h) = \left(h_{fix} + h_{trapeze}\right) \cdot \tan\beta \qquad (11)$$

$$W(h) = W_{Neg}(h) + W_{Pos}(h) \qquad (12)$$

The offset w is used as second alterable parameter to variate the calculated width $W(h)$. Fig. 7 shows the influence of different field of view parameter sets.

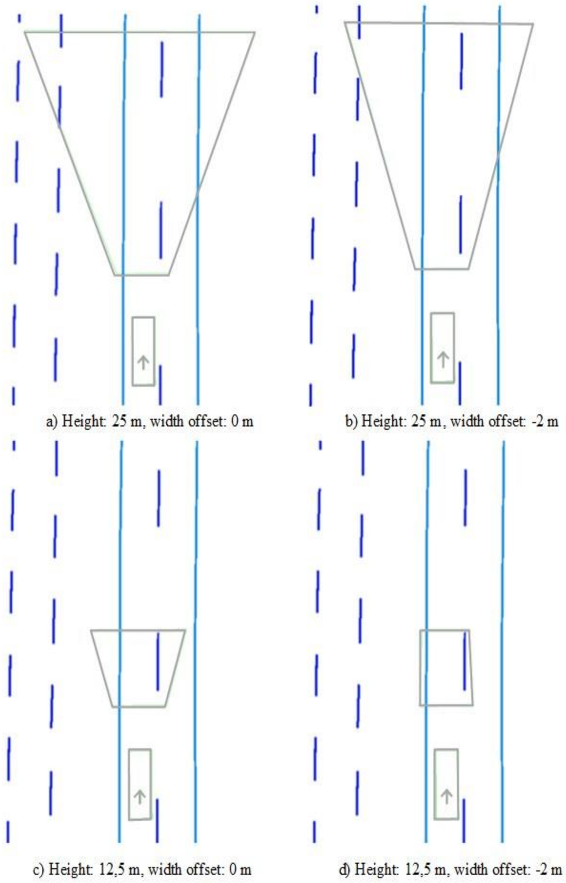

Figure 7. Different field of view configurations

To generate different parameter sets, we define start-, end and step values for both parameters. In the following h_s represents the start value for the trapeze height h_j, h_e represents the end value and h_{step} is the step size for each iteration. The width is defined similarly. For each h_j,w_j

$$h_j = h_s + j \cdot h_{step},\ j \in \mathbb{N}, h_j \in h_s, .., h_e \qquad (13)$$

and

$$w_j = w_s + j \cdot w_{step},\ j \in \mathbb{N}, w_j \in w_s, .., w_e \qquad (14)$$

hold true.

With this formula we get at most

$$c_h\left(h_s, h_e, h_{step}\right) = 1 + \frac{h_e\text{-}h_s}{h_{step}} \qquad (15)$$

$$c_w\left(w_s, w_e, w_{step}\right) = 1 + \frac{w_e\text{-}w_s}{w_{step}} \qquad (16)$$

$$c_t(h_s, h_e, h_{step} w_s, w_e, w_{step}) = c_h \cdot c_w \qquad (17)$$

An amount of $c_{t(h_s, h_e, h_{step}, w_s, w_e, w_{step})}$ parameter sets as shown from (15) to (17) has to be tested. An overturning trapeze with crossing vertices is not allowed. Consequently the effective amount of parameter sets is equal or less then the result of (17).

In order to get an optimal parameter set for one weather class we determine the effect on the localization quality for each set. The localization quality is defined as the average absolute distance between the corrected localization and a reference position.

We assume that optimal field of view parameters for different atmospheric conditions reduce the above mentioned distance better than a single set. As previous research has shown, different weather conditions negatively influence the localization accuracy [1], [11], [12].

To obtain the localization quality, we define a localization quality vector D , which contains the euclidean absolute distance d_i for each position measurement point i (see (18) and (19)). Each Di is equivalent to the longitudinal (δ_i^x) and lateral (δ_i^y) differences between the corrected localization and the reference position at the same point in time.

$$d_i(\delta_i^x, \delta_i^y) = \sqrt{(\delta_i^x)^2 + (\delta_i^y)^2} \qquad (18)$$

$$D = \begin{pmatrix} d_0 \\ d_1 \\ \cdots \\ d_n \end{pmatrix} \qquad (19)$$

Afterwards we calculate the average μ of D which defines the localization quality. Furthermore we assume that due to the continuity of environmental conditions the field of view parameter sets may lead to similar localization qualities. For this reason it is beneficial to identify appropriate regions of parameter sets. Of course, the parameter set with the lowest μ has to be part of this region. The region of appropriate parameter sets includes sets with similar localization quality. Thus, it is necessary to estimate the fluctuation of the set with the lowest average μ. Each parameter set the μ of which is within this fluctuation, is part of the appropriate parameter set region and others are discarded.

In order to approximate the fluctuation, we put each value i of D in one of ten bins by assigning i to the i mod 10-th bin. For each bin the average μ_i is calculated. Then, the standard deviation σ over all $\mu_i$is computed as in (20) presented.

$$\sigma = \sqrt{\frac{\sum_{i=1}^{10} \mu_i^2}{10} - \mu^2} \qquad (20)$$

The evaluation focuses on those parameter sets which are within two standard deviations.

We use the weighted average of the appropriate parameter sets $\text{para}_k^{\text{set}} = (\text{para}_k^{\text{height}}, \text{para}_k^{\text{width}})$ and interpret this as the optimal parameter set $\text{para}_{\text{opt}}^{\text{set}}$. The weighted average for each set k is thereby defined as

$$g_k(\mu_k) = \frac{1}{\mu_k} \qquad (21)$$

with $g_k(\mu_k)$ as the weight and μ_k as the set's average distance.

The number of appropriate parameter sets n with h_{opt} and w_{opt} is represented by $\text{para}_{\text{opt}}^{\text{set}}$as follows:

$$h_{opt} = \sum_{k=1}^{n} g_k(\mu_k) \cdot \text{para}_k^{\text{height}} \qquad (22)$$

$$w_{opt} = \sum_{k=1}^{n} g_k(\mu_k) \cdot \text{para}_k^{\text{width}} \qquad (23)$$

$$\text{para}_{\text{opt}}^{\text{set}} = (h_{opt}, w_{opt}) \qquad (24)$$

For each predefined weather class we use several test drives. Respectively we alter the field of view as described by (10) to (14). Then we apply (18) to (24) to determine the optimal parameter set. These sets then are averaged to compute the optimal parameter set for each atmospheric condition class.

IV. Experiments and Results

A. Preparation and Execution of Experiments

To start our evaluation, we make different test drives for each weather class. The used test vehicle is equipped with a Lidar, a front dash mono camera and an Applanix POS LV 510 System as reference system. During a test drive we collect and save all raw data. We have collected six drives for the wetness class, seven for the rain class and nine for the dryness class.

Figure 8. Urban 2.2 km long track from starting point A (52.423416, 10.748314) to ending point B (52.424257, 10.717625) in Wolfsburg, Germany

In our experiment we have used an urban 2.2km long road as shown in Fig. 8 from point A to B. All drives have been done under real traffic conditions but with the same traffic ratio.

The atmospheric conditions have been manually classified with meteorological data from a weather station near the track.

After all raw data has been collected, each test drive was simulated in several runs on a desktop machine. Within each run, a different parameter set was tested. . In each simulation run random noise was added to the reference position which was used as input for the memory and association module. The noise is based on the uncertainty of the LSDF position and has a Root

Mean Square (RMS) value of 0.75 meters for longitude and lateral position. The heading has a RMS of 0.5°. On average the input position has an inaccuracy of 1.5 meters which is equal to the typical uncertainty of the LSDF in urban areas.

Until now, the original field of view in the localization framework has been defined by the height value $h_{original}$ of 25m including h_{fix} and a width offset $w_{original}$ of 0m. The angles α and β are equally set to 24° which leads to a width of 11.1 m per side. We begin and end our field of view alterations with the following values:

$$h_s = 10m, h_e = 60m, h_{step} = 0.5m \quad (25)$$

$$w_s = 2.0m, w_e = -15.5m, w_{step} = -0.5m \quad (26)$$

B. Results

First we analyzed the field of view alterations for each test drive. Our findings for each drive show that different field of view parameters effect the localization quality that confirms our initial assumption. We have shown this behavior exemplary in Fig. 9 for one drive in the dryness. Here, all field of view parameter combinations are plotted. The localization quality is plotted along on the z-axis with ascending quality values in z-axis direction. The best result is shown as a black triangle on top. Additionally the expected field of view parameter set is depicted as black circle. It is easily seen that the expected set is far away from the best set concerning the parameters and particularly the localization quality.

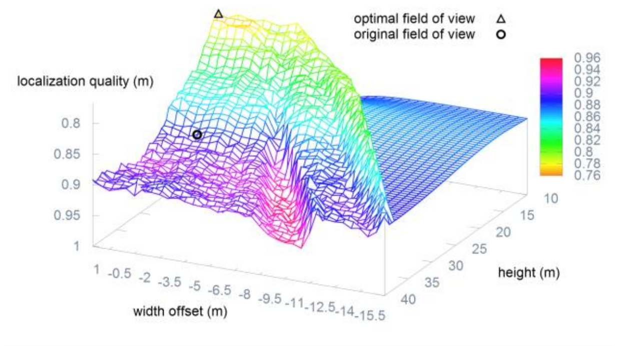

Figure 9. Localization quality for field of view alterations in one dryness drive

As the next step we analyzed the appropriate parameter sets for each drive in each atmospheric class respectively. With these values each drive's weighted parameter set $para_k^{set}$ (as shown in (21)) and $para_{opt}^{set}$ have been determined. For this we used the doubled standard deviation from (20). Subsequently we computed the average parameter set of each drive's optimum to receive the best set for the specific class.

The results are visualized from Fig. 10 to 12 for all weather classes. Hereby each drive's appropriate parameter sets are plotted with red dots. The dot size correlates to the localization quality, better quality leads to larger diameter. Each $para_k^{set}$ is represented by a black square. The average of all $para_k^{set}$ is $para_{opt}^{set}$ and is shown as black star. This is the estimated optimal field of view parameter set for this atmospheric condition.

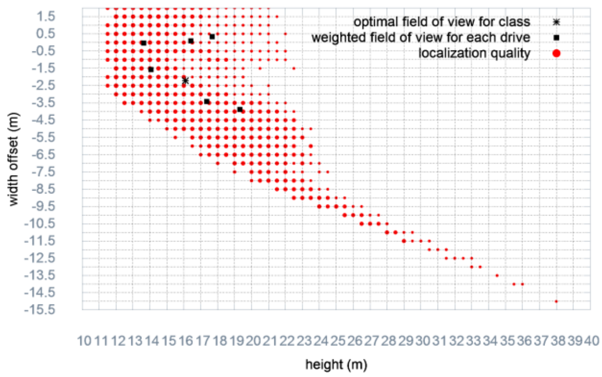

Figure 10. Field of view results for rain

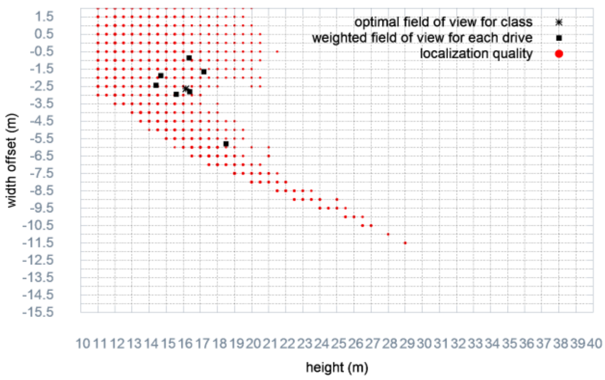

Figure 11. Field of view results for wetness

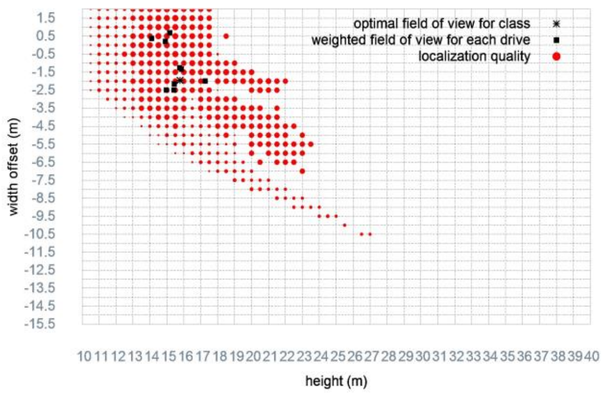

Figure 12. Field of view results for dryness

The final field of view for each class is shown in Fig. 13. Hereby the red broken dotted line symbolized the determined field of view for rain, the blue broken line stands for the field of view of the wetness class. For the dryness class a black dotted line is used to show the corresponding field of view. The beige box symbolizes the car with h_{fix} as starting point for the field of view and $h_{trapeze}$ as height for the field of view.

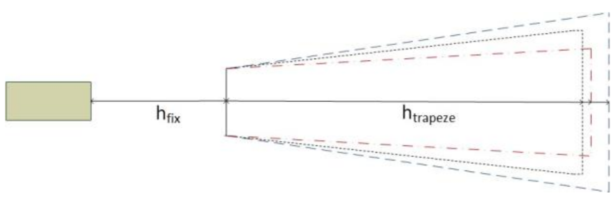

Figure 13. The optimal field of view for each weather class

TABLE I. DETERMINED FIELD OF VIEW VALUES FOR EACH WEATHER CLASS

Class	Field of view parameter		
	Width [m]	Height [m]	Area [m^2]
Rain	7,3	16,1	99,82
Wetness	10	16,4	123,82
Dryness	9,7	15,4	113,96

Table I outlines the determined field of view parameter set values for each atmospheric condition presented in Fig. 13. It can be seen that the parameter sets differentiate.

For a final test, we used test drives in each atmospheric condition which have not been considered to identify the optimal field of view parameter sets. In each category we run our localization framework with these test drives and the determined parameter sets from Table I. Furthermore, the LSDF absolute and relative car position estimates are used as input for the localization. The parameter sets presented here outperform the original field of view values in each class.

V. CONCLUSION

A method to generate field of view parameters for different atmospheric conditions has been presented. It has been assumed that results from a landmark based localization framework are correlated with the surrounding conditions and that the used modules can be parameterized for it. Contrary to prior research, we proposed a method to adjust the landmark based localization framework to the specified weather classes rain, wetness and dryness. Our results show that it is beneficial to find field of view parameters for each class. Also the transition from wetness to rain is smooth and hard to determine manually as proposed here, distinguished field of view parameter sets could be identified. In a first analysis the results showed that each identified field of view parameter set outperforms the origin one in the corresponding class.

In further work we want to improve our partitioning of the atmospheric conditions. Thus, the class wetness and rain will be divided into two classes each: low and high wetness as well as low and high rain. Also an improvement of the training set is needed. For that more drives in each class will be generated and used for the parameter exploration. Additionally, not only the field of view parameter should be determined for each class but also the tracking parameter within the memory module. By adjusting tracking parameters to the atmospheric conditions, better clutter handling might be reached. This topic will be also further investigated.

ACKNOWLEDGMENT

The authors would like to thank Laura-Kristin Rieche and Tobias Gärtner for their assistance.

REFERENCES

[1] F. B. Homm, “Fahrzeugeigenlokalisation im kontext hochautomatisierter fahrfunktionen,” Ph.D. dissertation, Technische Universität München, 2012.

[2] H. Lategahn and M. Schreiber, “Urban localization with camera and inertial measurement unit,” in *Proc. Intelligent Vehicles Symposium*, 2013, pp. 719–724.

[3] H. Lategahn and C. Stiller, “Experimente zur hochprazisen landmarkenbasierten eigenlokalisierung in unsicherheitsbehafteten digitalen karten,” in *Proc. Workshop Fahrerassistenzsysteme FAS*, 2012.

[4] S. Rauch and M. Aeberhard, “Autonomes fahren auf der autobahn - eine potentialstudie für zukünftige fahrerassistenzsysteme,” in *Proc. Tagung Fahrerassistenz*, 2012, pp. 1–13.

[5] H. Deusch, J. Wiest, and S. Reuter, “Multi-sensor selflocalization based on maximally stable extremal regions,” in *Proc. Intelligent Vehicles Symposium Proceedings*, 2014.

[6] M. Hentschel, O. Wulf, and B. Wagner, “A GPS and laser-based localization for urban and non-urban outdoor environments,” in *Proc. IEEE/RSJ International Conference on Intelligent Robots and Systems*, 2008, pp. 149–154.

[7] R. Krzikalla, A. Schindler, M. Wankerl, and R. Wertheimer, “Mehr sicherheit durch positionsbestimmung mit satelliten und landmarken,” *Vernetztes Automobil*, 2014.

[8] P. Muehlfellner, P. Furgale, W. Derendarz, and R. Philippsen, “Evaluation of fisheye-camera based visual multi-session localization in a realworld scenario,” in *Proc. Intelligent Vehicles Symposium*, 2013, pp. 57–62.

[9] T. Weiss, N. Kaempchen, and K. Dietmayer, “Precise ego-localization in urban areas using laserscanner and high accuracy feature maps,” in *Proc. Intelligent Vehicles Symposium*, 2005, pp. 284–289.

[10] T. Nothdurft, P. Hecker, S. Ohl, F. Saust, M. Maurer, A. Reschka, and J. Bohmer, “Stadtpilot: First fully autonomous test drives in urban traffic,” in *Proc. Intelligent Transportation Systems*, 2011, pp. 919–924.

[11] J. Levinson, M. Montemerlo, and S. Thrun, “Map-based precision vehicle localization in urban environments,” *Robotics: Science and Systems*, 2007.

[12] M. Roser and F. Moosmann, “Classification of weather situations on single color images,” in *Proc. Intelligent Vehicles Symposium*, 2008.

[13] H. Kurihata, T. Takahashi, and I. Ide, “Rainy weather recognition from in-vehicle camera images for driver assistance,” *Intelligent Vehicles C*, pp. 205–210, 2005.

[14] D. Fitzner, M. Sester, U. Haberlandt, and E. Rabiei, “Rainfall estimation with a geosensor network of cars-theoretical considerations and first results,” *Photogrammetrie-Fernerkundung - Geoinformation*, vol. 2013, no. 2, pp. 93–103, May 2013.

[15] M. Roser, *Modellbasierte und Positionsgenaue Erkennung von Regentropfen in Bildfolgen zur Verbesserung von Videobasierten Fahrerassistenzfunktionen*, KIT Scientific Publishing, 2012.

[16] M. Hentschel, “Langzeitnavigation mobiler Roboter in teilstrukturierten umgebungen auf basis eines raum-und zeitvarianten umgebungsmodells,” Ph.D. dissertation, Leibniz Universität Hannover, 2012.

[17] H. G. B. P. H. Tobias Scheide, Martin Escher, Ed., *Integere Fahrzeugortung für zukünftige Fahrerassistenzsysteme*, Deutsche Gesellschaft für Navigation. Darmstadt: POSNAV ITS, 2011.

Marek Stess was born in Kattowice, Poland, 1985. Mr. Stess received his M.Sc dgree in 2012 from the Leibniz Universität Hannover in Computer Science. Since 2013 Mr. Stess is working on his Ph. D. degree in the field of automated driving at Volkswagen AG in cooperation with the Leibniz Universität Hannover (Institue of System Engineering – Real Time Systems Group).

In 2008 he joined the Ricoh & Java Developer Challenge and reached the third. place. 2007 and 2008 he joined the Robot Day contest offered from SICK and reached the second place for the indoor contest and the third for the outdoor one. 2010 he was offered as awardee from the Leibniz Universität Hannover and 2011 from the German National Academic Foundation.